

Stripes in quasi two dimensional rare-earth tritellurides

Hong Yao, John A. Robertson, Eun-Ah Kim, and Steven A. Kivelson

Department of Physics, Stanford University, Stanford, CA 94305

(Dated: February 8, 2020)

Even though the rare-earth tritellurides are tetragonal materials with a quasi two dimensional (2D) band structure, they have a “hidden” 1D character. The resultant near-perfect nesting of the Fermi surface leads to the formation of a charge density wave (CDW) state. We show that for this band structure, there are two possible ordered phases: A bidirectional “checkerboard” state would occur if the CDW transition temperature were sufficiently low, whereas a unidirectional “striped” state, consistent with what is observed in experiment, is favored when the transition temperature is higher. This result may also give some insight into why, in more strongly correlated systems, such as the cuprates and nickelates, the observed charge ordered states are generally stripes as opposed to checkerboards.

I. INTRODUCTION

Many strongly correlated (layered) materials with quasi two dimensional (2D) structure show fluctuating or static stripe order (unidirectional density wave states) over a substantial range of temperatures.^{1,2,3} In particular, there has been considerable interest in studying whether or not stripes are inextricably connected to the high temperature superconductivity that occurs in the cuprates.^{1,2} However, characterizing the stripe order in these materials is difficult due to the complex and strongly correlated nature of these materials, and the presence of significant amounts of quenched disorder.⁴

From the symmetry view point, there is no difference between a unidirectional charge density wave state (CDW) in a weakly interacting quasi-2D system and a stripe-ordered state of a strongly correlated system. CDW states can occur in the weak coupling limit only if there are sufficiently well nested portions of the Fermi surface. Since this is non-generic in more than 1D, one would like to identify what is special about those higher dimensional materials in which nested Fermi surfaces appear. Moreover, for a layered quasi-2D material with tetragonal (C_4) symmetry, the CDW ground state can either be bidirectional (checkerboards) maintaining the point group symmetry of the lattice, or unidirectional (stripes) with a reduced symmetry, and again we would like to understand what physics governs this choice.

The rare-earth tritelluride series $R\text{Te}_3$ ($R=Y, \text{La-Tm}$) is particularly well suited for a detailed study of these issues. $R\text{Te}_3$ consists of square Te planes alternating with weakly coupled $R\text{Te}$ slabs. (See Fig. 2 of Ref. 5 for example.) The electronically active valence band derives from the $5p$ orbitals of the planar Te atoms, and is thus expected to be relatively weakly correlated. The existence of a unidirectional CDW was first detected by transmission electron microscopy (TEM).^{6,7} Angle resolved photoemission spectroscopy (ARPES)^{5,8,9} measurements have shown that the CDW ordering wavevector nests large portions of the Fermi surface, which are in turn gapped, thus strongly indicating that the CDW is a consequence of Fermi surface nesting. More recent X-ray scattering and STM measurements have confirmed the

existence of the CDW and its unidirectional character in great detail.^{10,11} Detailed studies of the Fermi surface topology using ARPES⁵ and positron annihilation¹² support the notion that the CDW is the result of a nesting-driven Fermi surface instability. However, the driving force for the strong breaking of the point group symmetry ($C_4 \rightarrow C_2$) produced by the unidirectional CDW formation in $R\text{Te}_3$ has not been clear previously.

We shall show in the present paper that the nesting of the Fermi surface of $R\text{Te}_3$ reflects a “hidden” 1D character of the electronic band structure which derives from the highly anisotropic hopping amplitude of the Te p_x and p_y orbitals.¹³ Consequently, CDW order occurs for a dimensionless effective interaction, λ , in excess of an extremely small critical value, $\lambda_c \ll 1$. (In 1D, the fact that $\lambda_c = 0$ is the famous Peierls instability.) Moreover, we shall show that there are two possible patterns of CDW order that can take best advantage of the nesting: checkerboard order that occurs for λ slightly larger than λ_c , and stripe order, which is also rotated relative to the checkerboard order, which occurs for $\lambda > \lambda_0 \approx \lambda_c[1 + \mathcal{O}(\lambda_c)]$; in more physical terms, what this means is that when the CDW transition temperature, T_c , or the CDW gap, Δ_0 , is sufficiently large, stripe order is favored. (The resulting phase diagram is shown in Fig. 4.)

II. BAND STRUCTURE CONSIDERATIONS

It is well established from transport measurements^{14,15} that the coupling between layers in $R\text{Te}_3$ is small. Comparisons between different rare earth compounds confirm the minor role of the rare earth in the electronic structure.^{5,15} Hence the physical properties of $R\text{Te}_3$ are dominantly determined by the Te planes common to all $R\text{Te}_3$. It is therefore natural to consider a simple model of the electronic structure of a single Te plane.

It is known, from first principle band structure calculations,¹⁶ that the energy of the $5p_z$ is shifted by crystal field effects so that it lies well below the Fermi energy. Consequently, the relevant bands close to the Fermi surface are the $5p_x$ and $5p_y$ orbitals, which are

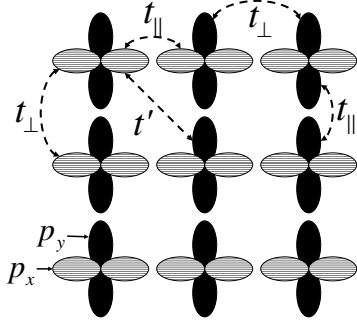


FIG. 1: The p_x (hatched) and p_y (solid) orbitals in the single Te square lattice. Due to the highly anisotropic profile of the p orbitals, the hopping amplitude, t_{\parallel} , along the extended direction of the given p orbital is much larger than the hopping amplitude t_{\perp} along the direction perpendicular to the extended direction. t' is a second-neighbor hopping, which is the shortest-range interaction which mixes the p_x and p_y bands, and which we neglect for present purposes.

approximately 5/8 filled. The crystallographic unit cell contains two Te atoms per plane due to a slight inequivalence between two sublattices produced by the $R\text{Te}$ slab orientation and the crystal structure is very weakly orthorhombic;¹² for simplicity, we will ignore these subtleties and consider an idealized Te square lattice. The band structure can be well approximated in the tight-binding approximation; the resulting Hamiltonian is shown schematically in Fig. 1.

Following Ref. 6, we neglect all interactions of longer-range than the nearest neighbor hopping, with the consequence that there is no hybridization between the p_x and p_y bands. (Small further neighbor interactions, such as the second neighbor hopping t' in Fig. 1, have a large effect on the Fermi surface topology where the two bands intersect, but can readily be shown to have little effect on the results obtained below.) Working in units where the lattice constant of the square lattice $a=1$, the dispersion for the p_x band and p_y band can be readily derived:

$$\begin{aligned} \epsilon_{\mathbf{k},p_x} &= -2t_{\parallel} \cos(k_x) + 2t_{\perp} \cos(k_y) \\ \epsilon_{\mathbf{k},p_y} &= 2t_{\perp} \cos(k_x) - 2t_{\parallel} \cos(k_y), \end{aligned} \quad (2.1)$$

where t_{\parallel} (t_{\perp}) represents the hopping amplitude parallel (perpendicular) to the extended direction of the given p orbital. Due to the highly anisotropic profile of the p orbital electron wave function, the hopping amplitude t_{\parallel} , along the extended direction of the given p orbital, is much larger than the hopping amplitude t_{\perp} perpendicular to the extended direction. Indeed these hopping amplitudes have been estimated¹⁶ to be $t_{\parallel} \approx 2.0\text{eV}$, $t_{\perp} \approx 0.37\text{eV}$, and $t' \approx 0.16\text{eV}$ for $R\text{Te}_3$. Thus, it is reasonable to set $t' = 0$ and to treat $t_{\perp}/t_{\parallel} \approx 0.18$ as a small parameter.

The small magnitude of the ratio t_{\perp}/t_{\parallel} implies a se-

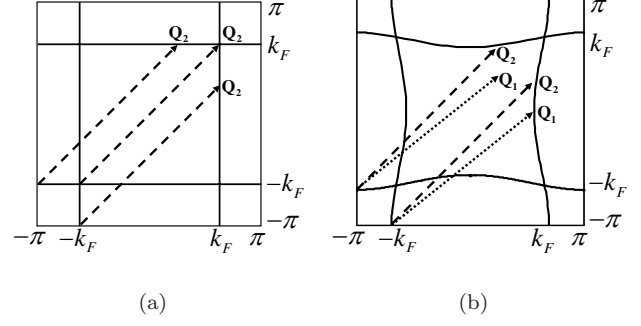


FIG. 2: Fermi surfaces (a) for $t_{\perp} = 0$ and (b) for t_{\perp} small, but non-zero. For $t_{\perp} = 0$, the wavevector $\mathbf{Q}_2 \equiv (2k_F, 2k_F)$ nests both the p_x -FS and the p_y -FS perfectly. For non-zero t_{\perp} , the wavevector $\mathbf{Q}_1 \equiv (2k_F, \pi)$ does a much better job of nesting the p_x -FS but a poor job on the p_y -FS. On the other hand, \mathbf{Q}_2 does a moderately good job of nesting the entire FS.

cret quasi-1D character of the band structure. For $t_{\perp} = 0$, the system would be equivalent to an array of 1D wires. Nonetheless, the system would maintain overall C_4 symmetry since these p_x and p_y “wires” are perpendicular to each other. Thus, even in this limit, the system would not display 2D anisotropy in any transport measurement. However, the resulting band structure would consist of two parallel 1D FS’s as shown in Fig. 2(a). With k_F defined by the implicit relation $\mu = -2t_{\parallel} \cos k_F$, where μ is the chemical potential, any wavevector $(\pm 2k_F, k_y)$ would then perfectly nest the p_x -FS for arbitrary k_y and wavevectors $(k_x, \pm 2k_F)$ would perfectly nest the p_y -FS for any k_x . In particular, the wavevectors $(\pm 2k_F, \pm 2k_F)$ perfectly nest both the p_x and p_y FS’s.

A small, but nonzero t_{\perp} introduces nonzero but small curvature to the FS (see Fig. 2(b)); the p_x -FS is determined by

$$k_x = \pm \left[k_F - \left(\frac{t_{\perp}}{t_{\parallel}} \right) \frac{\cos k_y}{\sin k_F} + \mathcal{O} \left(\frac{t_{\perp}^2}{t_{\parallel}^2} \right) \right], \quad (2.2)$$

where k_F is defined above. Here $+$ ($-$) represents the right (left) portion of the p_x -FS respectively. Obviously, the p_y -FS can be obtained from the p_x -FS by 90° rotation.

As a consequence of the finite curvature, the wavevector $(\pm 2k_F, k_y)$ nearly perfectly nests the p_x -FS *only for* $k_y = \pi$, and equivalently the p_y -FS is best nested by $(\pi, \pm 2k_F)$. However, away from the half filling, $(\pm 2k_F, \pi)$ does a poor job in nesting the p_y -FS and conversely for $(\pi, \pm 2k_F)$. Note that $(2k_F, \pi)$, $(-2k_F, \pi)$, $(\pi, 2k_F)$ and $(\pi, -2k_F)$ are related by the C_4 symmetry of the host lattice. On the other hand, the wavevector $(2k_F, 2k_F)$ (and its C_4 symmetry related vectors), which perfectly nests the full FS for $t_{\perp} = 0$, does a reasonable job in nesting both the p_x -FS and the p_y -FS. Thus, for small t_{\perp}/t_{\parallel} , there are two independent candidates (not related

to each other via C_4 symmetry) for the CDW ordering wavevectors:

$$\mathbf{Q}_1 \equiv (2k_F, \pi) \quad \text{and} \quad \mathbf{Q}_2 \equiv (2k_F, 2k_F). \quad (2.3)$$

To see which ordering vector is preferred, we now compute the corresponding charge density (Lindhard) susceptibility, $\chi(\mathbf{q}; T)$. For a given wavevector \mathbf{q} at a given temperature T ,

$$\chi(\mathbf{q}; T) = -2 \sum_{\eta} \int \frac{d\mathbf{k}}{(2\pi)^2} \frac{f(\xi_{\mathbf{k}\eta}, T) - f(\xi_{\mathbf{k}+\mathbf{q}\eta}, T)}{\xi_{\mathbf{k}\eta} - \xi_{\mathbf{k}+\mathbf{q}\eta}}, \quad (2.4)$$

where the integral is over the first Brillouin zone, $\eta = p_x, p_y$ is the band index, and $\xi_{\mathbf{k}\eta} = \epsilon_{\mathbf{k}\eta} - \mu$. The factor of 2 is from two spin polarizations of the electrons and $f(\xi_{\mathbf{k}\eta}, T)$ denotes the Fermi-Dirac distribution function.

For small t_{\perp}/t_{\parallel} , the susceptibilities at these two vectors have the following approximate analytical forms, which are valid for temperatures $T \ll t_{\perp}$ (in units $k_B = 1$):

$$\chi(\mathbf{Q}_1; T) \approx \rho(E_F) \log \left[\frac{\alpha_0 t_{\parallel}}{T + \alpha_1 t_{\perp}^2/t_{\parallel}} \right] + \rho(E_F) \log \left[\frac{\alpha_0 t_{\parallel}}{T + \alpha_2 t_{\parallel}} \right], \quad (2.5)$$

$$\chi(\mathbf{Q}_2; T) \approx 2\rho(E_F) \log \left[\frac{\alpha_0 t_{\parallel}}{T + \alpha_3 t_{\perp}} \right], \quad (2.6)$$

where $\rho(E_F) \equiv [2\pi t_{\parallel} \sin k_F]^{-1}$ is the density of states per spin per band and $\alpha_0 t_{\parallel}$ is the ultraviolet cutoff, which is of order of the bandwidth ($\alpha_0 \approx 2$). The parameters α_i are defined by

$$\begin{aligned} \alpha_1 &\approx |\cos k_F|/(4 \sin^2 k_F), \\ \alpha_2 &\approx 2|\cos k_F|, \\ \alpha_3 &\approx |\cos k_F|. \end{aligned} \quad (2.7)$$

In $R\text{Te}_3$, the bands are approximately $5/8$ filled, thus $k_F \approx 5\pi/8$. In the small but non-zero t_{\perp}/t_{\parallel} limit,

$$\chi(\mathbf{Q}_1; 0) \approx \chi(\mathbf{Q}_2; 0) + \rho(E_F) \log[2 \sin^2(k_F)]. \quad (2.8)$$

Therefore, if the CDW transition occurs at low enough temperatures the wavevector \mathbf{Q}_1 will be favored so long as $\pi/4 \lesssim k_F \lesssim 3\pi/4$. However, at high enough temperatures, $T > T_0 \sim t_{\perp}^2/t_{\parallel}$, $\chi(\mathbf{Q}_2; T)$ is greater than $\chi(\mathbf{Q}_1; T)$. Therefore, we expect there to be a finite temperature T_0 such that if the CDW transition temperature $T_c < T_0$, the ordering vector is $\mathbf{q} \approx \mathbf{Q}_1$, while for $T_c > T_0$, $\mathbf{q} \approx \mathbf{Q}_2$.

For a more quantitative analysis, we have numerically evaluated the susceptibility $\chi(\mathbf{q}; T)$ of Eq. (2.4), for wavevectors \mathbf{q} over the whole Brillouin zone. The calculated susceptibility has a maximum at a wavevector \mathbf{q}_{\max} close to \mathbf{Q}_1 or \mathbf{Q}_2 , depending on whether the temperature, $T < T_0$ or $T > T_0$, in agreement with our analysis of the FS. The precise location of \mathbf{q}_{\max} shifts slightly as

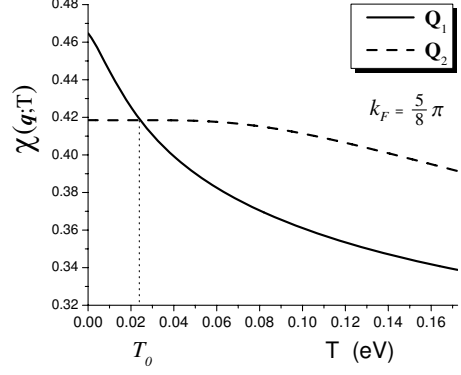


FIG. 3: The Linhard susceptibility $\chi(\mathbf{q}; T)$ as a function of T for $\mathbf{q} = \mathbf{Q}_1 \equiv (2k_F, \pi)$ and $\mathbf{q} = \mathbf{Q}_2 \equiv (2k_F, 2k_F)$.

a function of T , but so long as $T \ll t_{\parallel}$, the maximum always lies close to \mathbf{Q}_j , so this deviation does not significantly affect the resulting picture of the phase diagram. We will henceforth neglect this small effect, and focus our discussion on the wavevectors \mathbf{Q}_j . Fig. 3 shows the calculated $\chi(\mathbf{q}; T)$ for $\mathbf{q} = \mathbf{Q}_j$.

This result can be understood as follows: At low temperatures, the states arbitrarily close to the nearly perfectly nested portions of the Fermi surface dominate the susceptibility favoring \mathbf{Q}_1 . However, for $T > T_0$, the curvature of the FS has negligible effect, so \mathbf{Q}_2 is preferred. Since \mathbf{Q}_1 nests only the p_x portion of the FS, there is little competition between the ordering tendency at \mathbf{Q}_1 and at the symmetry related vector, $\bar{\mathbf{Q}}_1 = (\pi, 2k_F)$. Thus, as we shall show below, wherever CDW ordering with wavevector \mathbf{Q}_1 occurs, simultaneous ordering occurs at $\bar{\mathbf{Q}}_1 = (\pi, 2k_F)$, making this a state with “checkerboard” order. However, since ordering at wavevector \mathbf{Q}_2 opens a gap on the entire FS, it prevents ordering at the symmetry related vector, $\bar{\mathbf{Q}}_2 = (-2k_F, 2k_F)$; when \mathbf{Q}_2 is the preferred ordering vector, the resulting state has “stripe” order.

III. MEAN-FIELD PHASE DIAGRAM

To obtain an explicit phase diagram, we add an electron-phonon coupling and solve the resulting model in mean-field approximation. Thus, we investigate the following mean-field Hamiltonian

$$H_{MF} = \sum_{\mathbf{k}, \eta} \xi_{\mathbf{k}\eta} c_{\mathbf{k}\eta}^\dagger c_{\mathbf{k}\eta} + \sum_{\mathbf{q}} \frac{\rho(E_F)}{2\lambda_{\mathbf{q}}} |\Delta_{\mathbf{q}}|^2 + \sum_{\mathbf{k}, \mathbf{q}, \eta} \Delta_{\mathbf{q}} c_{\mathbf{k}+\mathbf{q}\eta}^\dagger c_{\mathbf{k}\eta}, \quad (3.1)$$

where the sum over \mathbf{q} runs over the possible ordering vectors, $\mathbf{q} = \pm\mathbf{Q}_1, \pm\bar{\mathbf{Q}}_1, \pm\mathbf{Q}_2$, and all harmonics, such as $\pm 2\mathbf{Q}_j$ and $\pm\mathbf{Q}_j \pm \bar{\mathbf{Q}}_j$. The order parameter $\Delta_{\mathbf{q}}$

for the CDW with the ordering vector \mathbf{q} is related to the lattice distortion $\langle x_{\mathbf{q}} \rangle$ through $\Delta_{\mathbf{q}} = \alpha_{\mathbf{q}} \langle x_{\mathbf{q}} \rangle$, where $\alpha_{\mathbf{q}}$ is the electron-phonon coupling, and the dimensionless effective interaction $\lambda_{\mathbf{q}} = [\alpha_{\mathbf{q}}^2 \rho(E_F)] / [M \omega_{\mathbf{q}}^2]$, where $\omega_{\mathbf{q}}$ is the phonon frequency and M is the ion mass. The self-consistent value of the gap is obtained by minimizing the free energy computed from H_{MF} with respect to $\Delta_{\mathbf{q}}$. Note that $\Delta_{-\mathbf{q}} = \Delta_{\mathbf{q}}^*$. We use the approximation $\lambda_{\mathbf{q}} = \lambda$ in the rest of this paper.

At high temperatures, clearly $\Delta_{\mathbf{q}} = 0$ for all \mathbf{q} . As the temperature is lowered, for sufficiently large λ , solutions with non-zero values of $\Delta_{\mathbf{q}}$ appear. In general, when $\Delta_{\mathbf{q}}$ is non-zero at some wavevector, \mathbf{q} , it is non-zero, although possibly much smaller, at all harmonics, as well.

For commensurate order, the mean-field equations can, in principle, be evaluated numerically exactly, but for high order commensurability this is quite a complicated problem, as there are many harmonics, and hence many possible patterns of order. For incommensurate order, even this is not possible.

Fortunately, in the present case, for the most part the transitions are continuous, or at worst weakly first order. Therefore, the phase boundaries can be identified by expanding the mean-field (Landau) free energy to low order in powers of $\Delta_{\mathbf{q}}$. The coefficients in this expansion are expressed as convolutions of free Green functions, as derived explicitly up to fourth order in the Appendix. To this order, only the fundamentals and their second harmonics enter the expansion; if \mathbf{q} and $\bar{\mathbf{q}}$ are two (symmetry related) fundamental ordering vectors, then the higher harmonics in powers of the fundamental, satisfy $\Delta_{n\mathbf{q}+m\bar{\mathbf{q}}} \sim [\Delta_{\mathbf{q}}^n \Delta_{\bar{\mathbf{q}}}^m]$. Indeed, in this context, we can treat the harmonics as slaves to the fundamentals and obtain a Landau free energy expressed exclusively in terms of $\Delta_{\mathbf{q}}$ and $\Delta_{\bar{\mathbf{q}}}$, as is done explicitly in the Appendix. The result is a free energy density

$$\mathcal{F} = \sum_{j=1}^2 \left[r_j (|\Delta_{\mathbf{Q}_j}|^2 + |\Delta_{\bar{\mathbf{Q}}_j}|^2) + \frac{u_j}{4} (|\Delta_{\mathbf{Q}_j}|^2 + |\Delta_{\bar{\mathbf{Q}}_j}|^2)^2 + \gamma_j |\Delta_{\mathbf{Q}_j}|^2 |\Delta_{\bar{\mathbf{Q}}_j}|^2 \right] + \dots, \quad (3.2)$$

where

$$r_j = \rho(E_F)/\lambda - \chi(\mathbf{Q}_j; T), \quad (3.3)$$

and ... signifies both higher order terms in powers of Δ , as well as unimportant biquadratic terms, such as $|\Delta_{\mathbf{Q}_1}|^2 |\Delta_{\mathbf{Q}_2}|^2$, which come into play only if ordering occurs both at $\mathbf{Q}_1 = (2k_F, \pi)$ and $\mathbf{Q}_2 = (2k_F, 2k_F)$. The coefficients u_j and γ_j are evaluated in the Appendix.

The mean-field phase diagram in Fig. 4 was constructed from this expression as follows: The phase boundaries were determined as the points at which either r_1 or r_2 vanishes, so both r_1 and $r_2 > 0$ in the high temperature phase. Throughout the ordered region of the phase diagram, we always find that $\gamma_1 < 0$ and $\gamma_2 > 0$, so wherever \mathbf{Q}_1 ordering is favored, simultaneous ordering at \mathbf{Q}_1 and $\bar{\mathbf{Q}}_1$, *i.e.*, checkerboard order, occurs, while in

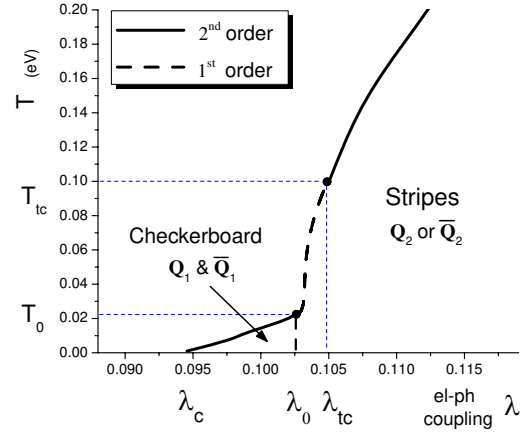


FIG. 4: The mean-field phase diagram. For $\lambda > \lambda_0$, the system orders to a stripe phase below the transition temperature. The associated phase transition is second order for $\lambda > \lambda_{tc}$ and first order for $\lambda_0 < \lambda < \lambda_{tc}$. For $\lambda_c < \lambda < \lambda_0$, the system orders to a checkerboard pattern. For $\lambda < \lambda_c$, there is no CDW instability down to zero temperature. Explicit numbers refer to the representative values of $t_{\parallel} = 2.0\text{eV}$, $t_{\perp} = 0.37\text{eV}$ and $k_F \approx 5\pi/8$.

the regions where \mathbf{Q}_2 ordering is favored, either $\Delta_{\mathbf{Q}_2}$ or $\Delta_{\bar{\mathbf{Q}}_2}$ is non-zero, but not both, *i.e.*, striped order occurs. The transition to the stripe phase is continuous so long as $u_2 > 0$, which is the case at large coupling. The tricritical point occurs where u_2 vanishes. Strictly speaking, where the transition becomes first order (the dashed lines in the figure), the Landau expansion is inadequate; the dashed lines should therefore be interpreted as schematic representations of the true phase boundaries. In evaluating the coefficients in the Landau expansion, we use the band structure with the representative values given in the caption of Fig. 4, but the phase diagram is qualitatively similar for any $t_{\perp} \ll t_{\parallel}$ and $\pi/4 \lesssim k_F \lesssim 3\pi/4$.

The main new physics apparent in this phase diagram arises from the sign of γ_j . The fact that γ_2 is robustly positive follows from the fact that \mathbf{Q}_2 does a moderately good job of nesting the entire FS; in the presence of a non-zero $\Delta_{\mathbf{Q}_2}$, most of the FS is gapped, so there are no remaining portions of the FS to be nested by $\bar{\mathbf{Q}}_2$. Conversely, the fact that \mathbf{Q}_1 fails so badly to nest the p_y portions of the FS, implies that there is no substantial interference between \mathbf{Q}_1 and $\bar{\mathbf{Q}}_1$ ordering; this leads to the expectation of a near vanishing biquadratic coupling, or in other words, $\gamma_1 \approx -u_1/2 < 0$, an expectation that we find is approximately satisfied. (At $T = 0$, $\gamma_1 \approx -25$ and $u_1 \approx 47$.)

Using the Landau free energy with coefficients given in the Appendix, for the band structure with the representative values, we can estimate the various critical values of the coupling constant: the minimum value for the existence of a CDW ground state is $\lambda_c \approx 0.093$; the critical value that separates the regime of checkerboard order from stripe order is $\lambda_0 \approx 0.103$; the tricritical coupling is $\lambda_{tc} \approx 0.105$; the temperature at the tricritical point

is $T_{tc} \approx 0.098$ eV. The maximum checkerboard ordering temperature, T_0 , which occurs on the edge of the first order transition to the striped phase, is the one qualitative feature of the phase diagram that depends on the higher order terms in the Landau expansion that we have not computed. The estimate for T_0 given in the figure comes from the assumption that the first order phase boundary lies close to the point at which r_2 vanishes.

IV. FLUCTUATION EFFECTS

We expect large fluctuation effects for the following reasons. It is common in CDW systems for the ratio of the zero temperature gap, Δ_0 , to the actual phase transition temperature, T_c , to be significantly larger than predicted by mean-field theory.^{17,18} On theoretical grounds, large fluctuation effects are characteristic of low dimensional systems. Moreover, in $R\text{Te}_3$, the ratio of the zero temperature gap to the bandwidth is not too small, $\Delta_0/(2t_{\parallel}) \approx 0.1$, in contrast with conventional superconductors, where the ratio is about 10^{-4} .

Whenever there is a large fluctuational suppression of T_c , local CDW correlations are expected to survive in a broad range of temperatures above T_c ; roughly, in the range $T_c < T < T_{MF}$, where $T_{MF} \approx \Delta_0/4$ is the mean-field transition temperature. One consequence of remaining local CDW correlations above T_c will be the presence of peaks in the structure factor at positions corresponding to the Bragg vectors of the ordered state, but with width inversely proportional to the thermal correlation length.¹⁹ However in the case of a stripe phase, more dramatic effects can be expected. If there is only a single transition, then the “stripe liquid” phase above T_c does not break any of the lattice symmetries, and consequently equivalent peaks in the structure factor should appear both at the stripe ordering vector, and at the conjugate wavevector (rotated by 90°). Such behavior has already been seen, albeit only in the magnetic scattering, in the stripe liquid phase of $\text{La}_{2-x}\text{Sr}_x\text{NiO}_4$.²⁰ On the other hand, a two stage transition is also possible with an intermediate, “stripe nematic” phase,²¹ in which stripe fluctuations are sufficiently violent to restore translation, but not the full C_4 symmetry of the host crystal; in such a phase, the peaks at the stripe ordering wave vector should be stronger (possibly, much stronger) than those at the conjugate wavevector. In this case, there must be a second transition at still higher temperatures to an isotropic state.

If future experiments can confirm the predictions above regarding the fluctuation effect, they will provide an important laboratory for exploring the physics of a stripe liquid, with possible broader implications to many stripy materials.

V. CONCLUDING REMARKS

The present mean-field theory gives results that are broadly consistent with experimental observation in $R\text{Te}_3$. The nature of the transition to the CDW state is unknown. However, from the value of the CDW gap measured by ARPES,^{5,8} one can estimate the mean-field transition temperature to be $T_{MF} \approx 0.11$ eV, which is an order of magnitude greater than the theoretical value of T_0 and also greater than T_{tc} . Hence, the theory predicts that $R\text{Te}_3$ should have a unidirectional CDW (stripes) ordered phase with ordering vector approximately equal to either $\mathbf{Q}_2 = (2k_F, 2k_F)$ or $\bar{\mathbf{Q}}_2 = (2k_F, -2k_F)$.²² This is consistent with the experiments^{5,6,8} which find stripe order with $\mathbf{Q}_{\text{CDW}} \approx (0.71\pi, 0.71\pi)$. Since $k_F \approx 5\pi/8$, the predicted magnitude of $\mathbf{Q}_2 \approx (0.75\pi, 0.75\pi)$ agrees with the measured \mathbf{Q}_{CDW} within 5 percent.

Charge density waves often break the point group symmetry of the host lattice. This phenomenon is particularly common in strongly correlated materials including many transition metal oxides which exhibit stripe order. The strong interactions present in those (d -band) systems make the physics of pattern selection more difficult to study from a microscopic viewpoint. However, one may hope that extrapolating from the weak coupling limit (solved in the present paper) may give some insight into the deeper issues of pattern selection in highly correlated materials.

The underlying physics that is responsible for the existence of a CDW state in the present class of reasonably weakly interacting quasi-2D systems is the existence of a hidden 1D character of the band structure. In the present paper, we have explored only the grossest aspects of this structure - those amenable to a mean-field analysis. At temperatures or frequencies in excess of the ordering temperature, where the band structure can be approximated as that of intersecting 1D systems, it is probable that more interesting fluctuation effects, associated with the breakdown of Fermi liquid theory in 1D, should be observable. Indeed, some evidence already exists²³ from high energy spectroscopies of anomalous power-law behaviors reminiscent of the 1D Luttinger liquid. We are currently exploring this aspect of the problem.

Acknowledgments We would like to thank S. Brown, A. Fang, I. R. Fisher, A. Kapitulnik, and N. Ru, for helpful discussions, and J. Allen and G.-H. Gweon for partially inspiring this work. This work was supported in part by NSF grant number DMR0531196 at Stanford University.

APPENDIX A: THE LINKED CLUSTER EXPANSION

Here we sketch the details of the linked cluster expansion that was used to obtain the coefficients of the GL

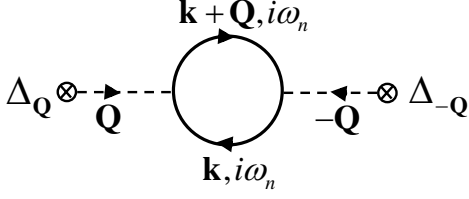


FIG. 5: The second order Feynman diagram from which we obtain the Lindhard susceptibility, $\chi_{\mathbf{Q}}$. Higher order diagrams differ only in the number of external legs.

free energy. We treat the off-diagonal part of the mean field Hamiltonian Eq. (3.1)

$$V = \sum_{\mathbf{k}, \mathbf{q}, \eta} \Delta_{\mathbf{q}} c_{\mathbf{k}+\mathbf{q}\eta}^\dagger c_{\mathbf{k}\eta} \quad (\text{A1})$$

as a perturbation to obtain the Landau free energy:

$$\mathcal{F}[\{\Delta_{\mathbf{q}}\}] = \mathcal{F}_0 + \sum_{\mathbf{q}} \frac{\rho(E_F)}{2\lambda} |\Delta_{\mathbf{q}}|^2 + \sum_{l=2}^{\infty} U_l[\{\Delta_{\mathbf{q}}\}], \quad (\text{A2})$$

where the set $\{\Delta_{\mathbf{q}}\}$ contains, in principle, all harmonics of the fundamental ordering vectors, although in practice we restrict ourselves to fourth order terms for the continuous phase transitions. The functionals, U_ℓ , are defined as

$$U_\ell = \frac{(-1)^{\ell+1}}{\ell} \frac{1}{\beta} \int_0^\beta d\tau_1 \cdots \int_0^\beta d\tau_\ell \langle T_\tau V(\tau_1) \cdots V(\tau_\ell) \rangle. \quad (\text{A3})$$

The expansion in terms of U_ℓ contains only fully connected, 1-loop diagrams, where the finite-temperature Green functions for the electrons are

$$\mathcal{G}_0^\eta(\mathbf{k}, \omega_n) = \frac{1}{i\omega_n - \xi_{\mathbf{k}\eta}}, \quad (\text{A4})$$

with $\omega_n = (2n+1)\pi/\beta$, and the order parameters, $\Delta_{\mathbf{Q}}$, act as external, single-particle potentials (see, for example, Fig. 5).

To fourth order, the Landau free energy in terms of order parameters associated with \mathbf{Q}_1 , \mathbf{Q}_2 and their harmonics is

$$\begin{aligned} \mathcal{F} = \mathcal{F}_0 &+ \sum_{j=1}^2 \left\{ r_j (|\Delta_{\mathbf{Q}_j}|^2 + |\Delta_{\bar{\mathbf{Q}}_j}|^2) + \bar{r}_j (|\Delta_{2\mathbf{Q}_j}|^2 + |\Delta_{2\bar{\mathbf{Q}}_j}|^2) + \tilde{r}_j (|\Delta_{\mathbf{Q}_j+\bar{\mathbf{Q}}_j}|^2 + |\Delta_{\mathbf{Q}_j-\bar{\mathbf{Q}}_j}|^2) + d_j (|\Delta_{\mathbf{Q}_j}|^4 + |\Delta_{\bar{\mathbf{Q}}_j}|^4) \right. \\ &\left. + g_j |\Delta_{\mathbf{Q}_1}|^2 |\Delta_{\mathbf{Q}_2}|^2 + [b_j (\Delta_{\mathbf{Q}_j}^2 \Delta_{-2\mathbf{Q}_j} + \Delta_{\bar{\mathbf{Q}}_j}^2 \Delta_{-2\bar{\mathbf{Q}}_j}) + c_j (\Delta_{\mathbf{Q}_j} \Delta_{\bar{\mathbf{Q}}_j} \Delta_{-\mathbf{Q}_j-\bar{\mathbf{Q}}_j} + \Delta_{\mathbf{Q}_j} \Delta_{-\bar{\mathbf{Q}}_j} \Delta_{\bar{\mathbf{Q}}_j-\mathbf{Q}_j}) + \text{c.c.}] \right\}, \quad (\text{A5}) \end{aligned}$$

where the coefficients are given by the integrals

$$r_j = \rho(E_F)/\lambda - \chi(\mathbf{Q}_j; T) \quad (\text{A6})$$

$$\bar{r}_j = \rho(E_F)/\lambda - \chi(2\mathbf{Q}_j; T) \quad (\text{A7})$$

$$\tilde{r}_j = \rho(E_F)/\lambda - \chi(\mathbf{Q}_j + \bar{\mathbf{Q}}_j; T) \quad (\text{A8})$$

$$b_j = \int' \mathcal{G}_0^\eta(0) \mathcal{G}_0^\eta(\mathbf{Q}_j) \mathcal{G}_0^\eta(2\mathbf{Q}_j) \quad (\text{A9})$$

$$c_j = \int' \left\{ \mathcal{G}_0^\eta(0) \mathcal{G}_0^\eta(\mathbf{Q}_j) \mathcal{G}_0^\eta(\mathbf{Q}_j + \bar{\mathbf{Q}}_j) + \mathcal{G}_0^\eta(0) \mathcal{G}_0^\eta(\bar{\mathbf{Q}}_j) \mathcal{G}_0^\eta(\mathbf{Q}_j + \bar{\mathbf{Q}}_j) \right\} \quad (\text{A10})$$

$$d_j = \int' \left\{ \mathcal{G}_0^\eta(0) \mathcal{G}_0^\eta(\mathbf{Q}_j)^2 \mathcal{G}_0^\eta(2\mathbf{Q}_j) + \frac{1}{2} \mathcal{G}_0^\eta(0)^2 \mathcal{G}_0^\eta(\mathbf{Q}_j)^2 \right\} \quad (\text{A11})$$

$$\begin{aligned} g_j = \int' &\left\{ \mathcal{G}_0^\eta(0)^2 \mathcal{G}_0^\eta(\mathbf{Q}_j) \mathcal{G}_0^\eta(\bar{\mathbf{Q}}_j) + \mathcal{G}_0^\eta(0)^2 \mathcal{G}_0^\eta(\mathbf{Q}_j) \mathcal{G}_0^\eta(-\bar{\mathbf{Q}}_j) + \mathcal{G}_0^\eta(0) \mathcal{G}_0^\eta(\mathbf{Q}_j)^2 \mathcal{G}_0^\eta(\mathbf{Q}_j + \bar{\mathbf{Q}}_j) \right. \\ &\left. + \mathcal{G}_0^\eta(0) \mathcal{G}_0^\eta(\mathbf{Q}_j)^2 \mathcal{G}_0^\eta(\mathbf{Q}_j - \bar{\mathbf{Q}}_j) + 2 \mathcal{G}_0^\eta(0) \mathcal{G}_0^\eta(\mathbf{Q}_j) \mathcal{G}_0^\eta(\bar{\mathbf{Q}}_j) \mathcal{G}_0^\eta(\mathbf{Q}_j + \bar{\mathbf{Q}}_j) \right\}, \quad (\text{A12}) \end{aligned}$$

and we have adopted the compactified notation:

$$\mathcal{G}_0^\eta(\mathbf{q}) \equiv \mathcal{G}_0^\eta(\mathbf{k} + \mathbf{q}, i\omega_n) \quad (\text{A13})$$

$$\int' \equiv 2 \sum_{\eta} \frac{1}{\beta} \sum_{i\omega_n} \int \frac{d\mathbf{k}}{(2\pi)^2}. \quad (\text{A14})$$

As the susceptibility towards ordering is always largest for the fundamental vectors, we integrate out the higher harmonics, which allows us to write the free energy in a form that transparently displays the C_4 symmetry of the

problem

$$\mathcal{F} = \sum_j [r_j(|\Delta_{\mathbf{Q}_j}|^2 + |\Delta_{\bar{\mathbf{Q}}_j}|^2) + \frac{u_j}{4}(|\Delta_{\mathbf{Q}_j}|^2 + |\Delta_{\bar{\mathbf{Q}}_j}|^2)^2 + \gamma_j|\Delta_{\mathbf{Q}_j}|^2|\Delta_{\bar{\mathbf{Q}}_j}|^2]. \quad (\text{A15})$$

The effect of higher harmonics is to renormalize the co-

efficients of the quartic terms, which become

$$u_j = 4(d_j - |b_j|^2/\tilde{r}_j) \\ \gamma_j = g_j - |c_j|^2/\tilde{r}_j - u_j/2. \quad (\text{A16})$$

-
- ¹ J. M. Tranquada, H. Woo, T. G. Perring, H. Goka, G. D. Gu, G. Xu, M. Fujita, and K. Yamada, *Nature* **429**, 534 (2004).
- ² S. A. Kivelson, I. P. Bindloss, E. Fradkin, V. Oganessian, J. M. Tranquada, A. Kapitulnik, and C. Howald, *Rev. Mod. Phys.* **75**, 1201 (2003).
- ³ M. P. Lilly, K. B. Cooper, J. P. Eisenstein, L. N. Pfeiffer, and K. W. West, **82**, 394 (1999).
- ⁴ J. Robertson, S. A. Kivelson, E. Fradkin, A. Fang, and A. Kapitulnik, *cond-mat/0602675*.
- ⁵ V. Brouet, W. L. Yang, X. J. Zhou, Z. Hussain, N. Ru, K. Shin, I. R. Fisher, and Z. X. Shen, *Phys. Rev. Lett.* **93**, 126405 (2004).
- ⁶ E. Dimasi, M. C. Aronson, J. F. Mansfield, B. Foran, and S. Lee, *Phys. Rev. B* **52**, 14516 (1995).
- ⁷ E. DiMasi, B. Foran, M. C. Aronson, and S. Lee, *Phys. Rev. B* **54**, 13587 (1996).
- ⁸ G.-H. Gweon, J. D. Denlinger, J. A. Clack, J. W. Allen, C. G. Olson, E. DiMasi, M. Aronson, B. Foran, and S. Lee, *Phys. Rev. Lett.* **81**, 886 (1998).
- ⁹ H. Komoda, T. Sato, S. Souma, T. Takahashi, Y. Ito, and K. Suzuki, *Phys. Rev. B* **70**, 195101 (2004).
- ¹⁰ H. J. Kim, C. D. Malliakas, A. Tomic¹, S. H. Tessmer¹, M. G. Kanatzidis, and S. J. L. Billinge, *Phys. Rev. Lett.* **96**, 226401 (2006).
- ¹¹ A. Fang, N. Ru, I. R. Fisher, and A. Kapitulnik, to be published.
- ¹² J. Laverock, S. B. Dugdale, Z. Major, M. A. Alam, N. Ru, I. R. Fisher, G. Santi, and E. Bruno, *Phys. Rev. B* **71**, 085114 (2005).
- ¹³ Another example of a 2D metal with a unidirectional CDW is the purple bronze η - Mo_4O_{11} . It is now well known that this material has hidden 1D character related to the presence of conducting chains.^{24,25,26,27} Since there are chains running along three different directions, the system as a whole has hexagonal symmetry. Indeed, the present work was, in part, inspired by the earlier work of Gweon *et al*, Ref. 27. However, there are no chain-like structural units in RTe_3 .
- ¹⁴ E. DiMasi, B. Foran, M. C. Aronson, and S. Lee, *Chem. Mater.* **6**, 1867 (1994).
- ¹⁵ N. Ru and I. R. Fisher, *Phys. Rev. B* **73**, 033101 (2006).
- ¹⁶ A. Kikuchi, *J. Phys. Soc. Jpn* **67**, 1308 (1998).
- ¹⁷ D. C. Johnston, M. Maki, and G. Gruner, *Solid State Communication* **53**, 5 (1985).
- ¹⁸ R. S. Kwok, G. Gruner, and S. E. Brown, *Phys. Rev. Lett.* **65**, 365 (1990).
- ¹⁹ S. Girault, A. H. Moudden, and J. P. Pouget, *Phys. Rev. B* **39**, 4430 (1989).
- ²⁰ S.-H. Lee, J. M. Tranquada, K. Yamada, D. J. Buttrey, Q. Li, and S.-W. Cheong, *Phys. Rev. Lett.* **88**, 126401 (2002).
- ²¹ S. A. Kivelson, E. Fradkin, and V. J. Emery, *Nature (London)* **393**, 550 (1998).
- ²² There is a small orthorhombicity in the crystal structure, which therefore acts as a weak symmetry breaking field. Thus, rather than domains of different orientation stripes, which might otherwise be expected, stripe order with a single ordering vector (\mathbf{Q}_2 , not $\bar{\mathbf{Q}}_2$) is stabilized.
- ²³ A. Sacchetti, L. Degiorgi, T. Giamarchi, N. Ru, and I. R. Fisher, to be published.
- ²⁴ M. H. Whangbo, E. Canadell, P. Foury, and J. P. Pouget, *Science* **252**, 96 (1991).
- ²⁵ M. Braden, O. Friedt, Y. Sidis, P. Bourges, M. Minakata, and Y. Maeno, *Phys. Rev. Lett.* **88**, 197002 (2002).
- ²⁶ S. Hill, S. Uji, M. Takashita, C. Terakura, T. Terashima, H. Aoki, J. S. Brooks, Z. Fisk, and J. Sarrao, *Phys. Rev. B* **58**, 10778 (1998).
- ²⁷ G.-H. Gweon, S.-K. Mo, J. W. Allen, C. R. Ast, H. Höchst, J. L. Sarrao, , and Z. Fisk, *Phys. Rev. B* **72**, 35126 (2005).